## Fast Text-Conditional Discrete Denoising on Vector-Quantized Latent Spaces

Dominic Rampas<sup>§</sup>
Technische Hochschule Ingolstadt
Ingolstadt, Germany
and
Wand Technologies Inc.
New York, USA

dominic.rampas@gmail.com

Pablo Pernias§ Independent Researcher Sant Joan d'Alacant, Spain

pablo@pernias.com

Elea Zhong Wand Technologies Inc. New York, USA

eleaz@usc.edu

Marc Aubreville Technische Hochschule Ingolstadt Ingolstadt, Germany

marc.aubreville@thi.de



Figure 1: Visual results of our proposed method and trained model called *Paella*. It is able to perform a variety of image synthesis tasks. The left-hand side shows our model's abilities on text-conditional image generation on different sizes while the right side shows different other image synthesis tasks such as variations of images, latent space interpolation, structural editing, and outpainting.

## **Abstract**

Conditional text-to-image generation has seen countless recent improvements in terms of quality, diversity and fidelity. Nevertheless, most state-of-the-art models require numerous inference steps to produce faithful generations, resulting in performance bottlenecks for end-user applications. In this paper we introduce Paella, a novel text-toimage model requiring less than 10 steps to sample highfidelity images, using a speed-optimized architecture allowing to sample a single image in less than 500 ms, while having 573M parameters. The model operates on a compressed & quantized latent space, it is conditioned on CLIP embeddings and uses an improved sampling function over previous works. Aside from text-conditional image generation, our model is able to do latent space interpolation and image manipulations such as inpainting, outpainting, and structural editing. We release all of our code and pretrained models at https://github.com/dome272/Paella.

## 1 Introduction

Recent research in text-to-image generation [12, 29, 34, 31] has yielded stunning progress in terms of diversity, quality, and variation of generated images. The impressive output quality of these models, however, has come with the tradeoff that they require many sampling steps, leading to slow inference speeds unideal for end-user applications. Most current state-of-the-art works either rely on diffusion models [16] or are transformer [41]-based. Transformers usually employ a spatial compression to a lowdimensional space before learning, which is necessary due to the self-attention mechanism growing quadratically with latent space dimensions [5]. Furthermore, a transformer treats images as one-dimensional sequences by flattening the encoded image tokens, which is an unnatural projection of images and requires a significantly higher model complexity to learn an understanding of the 2D structure of images. The auto-regressive nature of transformers also re-

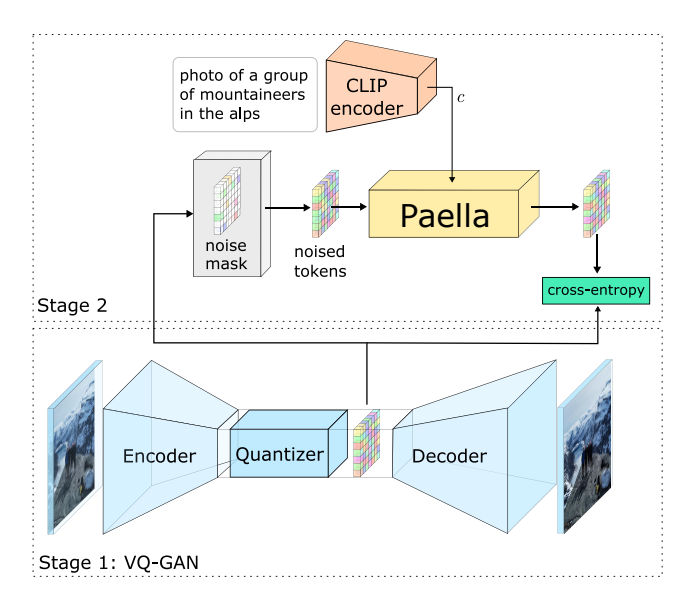


Figure 2: Visual depiction of the overall architecture of our proposed method. Training of *Paella* operates on a compressed latent space. Latent images are noised and the model is optimized to predict the unnoised version of the image.

quires to sample each token one at a time, resulting in long sampling times and high computational costs. On the other hand, diffusion models can effectively learn at the pixel level, yet, by default require a tremendously high number of sampling steps as well.

In this work, we propose a novel technique for textconditional image generation which is neither transformernor diffusion-based, but utilizes a fully convolutional neural network architecture. With our model, we can sample images with as few as 8 steps while still achieving high-fidelity results, making the model attractive for use-cases that are limited by requirements on latency, memory or computational complexity. Our model operates on a quantized latent space (see Figure 2) and employs a Vector-quantized Generative Adversarial Network (VQGAN) [11] for the encoding and decoding process with a moderate compression rate. Theoretically, we can use a much lower compression rate due to the convolutional nature of our model, which is not constrained by typical transformer limitations such as quadratic memory growth. A low compression rate allows to preserve fine details that are usually lost when working with higher compression. During training we quantize images using the aforementioned VOGAN and randomly noise the image tokens. The model is tasked to reconstruct the image tokens given the noised version and a conditional label. Sampling new images happens in an iterative fashion and is inspired by Masked Generative Image Transformer (MaskGIT) [4], but with significant changes: Chang et al.include a special mask token and use it to, initially, mask the full image. Then, the model iteratively predicts all tokens in the image simultaneously but keeps only a certain number of tokens which the model is the most confident about, while the rest of the tokens are masked again. We argue that this procedure is very restrictive in that it does not allow the model to self-correct its predictions at early steps during sampling. In order to provide more flexibility to the model, we randomly noise tokens instead of masking them. This gives the model the opportunity to refine its predictions for certain tokens over the course of sampling. Moreover, we improve sampling by using Classifier-Free Guidance (CFG) [18, 25], which is achieved by randomly performing unconditional training. To improve the sampling process we also use Locally Typical Sampling (LTS) [24]. We enable text conditioning by using Contrastive Language-Image Pretraining (CLIP) embeddings [26] as proposed by Wang et al.and Ramesh et al. [42, 29], however instead of solely training on image embeddings and subsequently learning a prior network for mapping text embeddings to image embeddings, we only train on text embeddings which decouples our model from the dependency on an explicit prior [31] and reduces computational complexity. Due to the fact that our model is fully convolutional it can generate images at any size, in principle. This property can be used for outpainting images (Figures 1 and 9), while still only requiring to sample once. Transformers need to shift the context window iteratively to generate larger-sized latent resolutions for this ability, which comes with quadratically growing sampling times. Besides outpainting an image, we can also do text-guided inpainting (Figure 10). Moreover, the ability to generate variations of images can be made possible by finetuning our model on image embeddings (Figure 8). Furthermore, the usage of CLIP embeddings enables us to do latent space interpolations (Figures 11). Lastly, multi-conditioning is possible too 13) and structural editing from a given base image (Figure 12).

Our main contributions are the following:

- 1. We propose a novel training objective for text-toimage generation based upon discrete (de)-noising in a quantized vector space, which uses a parameterefficient fully convolutional network.
- We introduce a simplified and improved sampling scheme over previous work, which is capable of sampling high quality images using a small number of steps.
- We explore the capabilities of our proposed scheme for image variations, inpainting & outpaiting, latent space interpolation, multi-conditioning and structural editing.

#### 2 Related Work

#### 2.1 Image Generation

Generative Adversarial Networks (GANs) are models which utilize a generator model and a discriminator model to create realistic samples following a desired data distribution. In image processing, GANs are commonly built using a convolutional architecture. The min-max optimization between both models allows them to generate high-fidelity images [3]. Their convolutional architecture allows them to both capture the 2D nature of images, as well as to scale linearly with the total number of pixels. However, GANs suffer from well-known problems such as mode collapse and convergence failure, making them hard to train without careful selection of hyper-parameters and suitable training objectives, which additionally complicates adaptation to novel domains [2, 1]. As language models started utilizing attention and the transformer architecture [41] became dominant, it was soon also applied in the field of computer vision [5, 27], with vision transformers [10] excelling in image comprehension, and ImageGPT [5] showing success in small image generation by using a transformer to discretely model the pixel space. ImageGPT treats pixels as individual tokens, and generates tokens in an autoregressive manner, from left to right and top to bottom. Yet, the quadratic memory growth of transformers with its input size, has limited this approach to small scales. In recent literature, a novel type of image generation framework called diffusion [16, 38] has matched and even surpassed GANs in conditional and unconditional image generation [7]. Diffusion models, propose a likelihood-based model, iteratively removing noise from a target image, where the training objective is expressed as a reweighted variational lower-bound. Recent work has shown that diffusion models can be scaled to high resolutions using multi-stage approaches, while maintaining the ability to generate highfidelity images [34, 29].

#### 2.2 Two Stage Approaches

Recent image generation models [11, 12, 30, 8] often utilize a two-stage approach, combatting limitations of the transformer model architecture, allowing for much higher resolution synthesis without creating unreasonably large models. These models use a Vector-quantized Variational Autoencoder (VQ-VAE) [40] to encode an image into discrete tokens, allowing for an autoregressive model to generate tokens which are subsequently decoded by the VQ-VAE. Many innovative approaches have originated from this style of model, often using tokens in GPT modeling space, to encode pertinent data. For instance, Make-a-Scene by Gafni *et al.*[12], applies a separate VQ-VAE to encode segmen-

tation maps of images, which are used as additional conditioning information for the image generation process. Other approaches [9, 4] use a bidirectional transformer to combat problems which are present in autoregressive models. For example, image generation can happen using only a fraction of the steps, while also being able to use a global context during generation and inpainting. In order to enable bidirectionality, Ding *et al.*[8] still employ an auto-regressive-like approach, while MaskGIT [4] generates all tokens at once, filtering for the highest confident ones and re-masking lower-confidence tokens at every iteration. Another successful work by Rombach *et al.*[31] discarded transformers in the vector-quantized latent space and replaced it by diffusion models.

One relevant property in two-stage models is the compression level of the first-stage model (often a VQ-VAE). Higher compression levels will often result in less clear and less accurate generations, while lower compression allows for very accurate reconstructions. But, because the length of the latent tokens determines the size (and speed) of the model, many previous works trade off lower latent space resolution for higher image resolution, higher fidelity, and larger model size.

#### 2.3 CLIP Guidance

CLIP [26] is a contrastive multimodal model which aims to align semantically similar textual descriptions and images in a shared latent space, allowing for zero-shot classification of image datasets, providing a much higher generalization ability than typical image classification approaches. Many recent approaches for image generation have relied on a frozen CLIP model as their sole method of conditioning. Dalle-2 by Ramesh et al. [29] only uses CLIP image embeddings as the input to their diffusion model, while relying on a "prior" converting CLIP text embeddings to image embeddings to enable text-to-image synthesis. However, work by Saharia et al.[34] finds that using a unimodal large language model (T5 [28]) can encode textual prompts better than CLIP, resulting in more accurate depictions of the textual prompts. Recent improvements by Rombach et al.to latent diffusion models also uses CLIP as their sole conditioning model, while providing high quality generation results [31].

#### 3 Method

#### 3.1 Token Predictor Optimization

Our proposal builds on the two-stage paradigm introduced by Esser *et al.*[11] and consists of a VQGAN for projecting the high-dimensional images into a lower-dimensional latent space, as shown in Figure 2. Specifi-

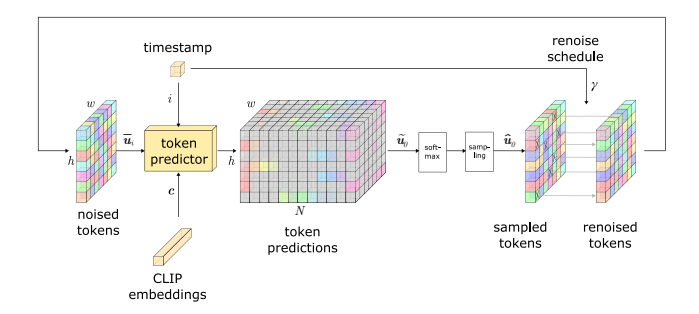


Figure 3: Training and sampling mechanism for the token predictor of our model.

cally, an encoder takes in the image at its base resolution of  $H \times W \times C$  and maps it to a latent representation  $\mathbf{u}$  with a resolution of  $h \times w \times z$  with h = H/f, w = W/f, where f is the compression rate. This operation is followed by a quantization step, replacing each vector by its nearest neighbour from a learned codebook  $Q \in \mathbb{R}^{N \times z}$  of size N. Afterwards, the quantized representation is given to the decoder which tries to reconstruct the input image. We use a pretrained VQGAN with an f=8 compression and a base resolution of  $256 \times 256 \times 3$ , mapping the image to a latent resolution of  $32 \times 32 \times 256$ .

The second stage learns the distribution of tokens in images in the low-dimensional latent space. During training we noise the latent tokens from the encoded and quantized images by randomly replacing some portion of the tokens with other randomly selected tokens from the codebook, as shown in Figure 3. The exact amount of noised tokens is determined by a scheduling function  $\gamma$  as proposed by Chang et al.[4]. As them, we also use a cosine schedule  $s(t) \in (0,1]$ . At training, a random number  $t \sim \mathcal{U}(0,1)$  is generated for each image and given to the schedule which returns the percentage of tokens to be noised s(t). We then sample a binary noise mask m with elements  $m_{x,y}$ , using a Bernoulli distribution with the probability for each position in the mask being s(t). The noised tokens  $\bar{u}_{x,y}$  at coordinate (x, y) are then drawn from a uniform distribution  $n_{x,y} \sim \mathcal{U}(0, N-1)$  as:

$$\bar{u}_{x,y} = \begin{cases} u_{x,y} & \text{if} \quad m_{x,y} = 1\\ n_{x,y} & \text{else} \end{cases}$$

The noised image representation  $\bar{\mathbf{u}}$  is then fed to the token prediction model  $f_{\theta}$  together with two more quantities: the timestep t and a condition c. As in diffusion models [16], we decided to include the current timestep in the model's input to provide an explicit source of information to the model of how much noise is present in the image and how much it is expected to remove. Moreover, we condition the model on this extra information, which we include in every layer, via linear projections. While any condition can

be included, such as class labels or semantic segmentation maps, we decided to condition the model on CLIP [26] embeddings. The noised indices, the timestep embedding and the CLIP embedding are given as input to the token predictor model which is tasked to predict the un-noised tokens, yielding a prediction  $\tilde{\mathbf{u}} \in \mathbb{R}^{h \times w \times N}$ .

$$\tilde{\mathbf{u}} = f_{\theta}(\bar{\mathbf{u}}, \mathbf{c}, \mathbf{t})$$

The token predictor is optimized via cross-entropy using label smoothing.

## 3.2 Sampling

While sampling in a single step would technically be possible, this procedure does not align properly with the training objective, as pointed out by [4]. Therefore, we also decided to use an iterative approach for sampling. Let  $\mathbf{u}_T \in \mathbb{N}_0^{h \times w}$  be a latent image where each value is a random token from the codebook. Furthermore, let  $\mathbf{t} = [t_T, t_{T-1}, \ldots, t_1]$  be the sequence of timesteps starting at  $t_T = 1$  (fully noised) and  $t_1 = \frac{1}{T}$  (almost noise-free) with T being the number of sampling steps. Moreover,  $\mathbf{c} \in \mathbb{R}^d$  denotes the CLIP embedding. Sampling is conducted in an iterative fashion and the following steps are executed in each iteration:

- (i) The current time-step  $i \in \mathbf{t}$ , the latent space representation of the input  $\mathbf{u}_i$ , and the embedding  $\mathbf{c}$  is given as input to the denoising model and it will predict all tokens simultaneously resulting in a score for each codebook index for the entire latent image. Specifically, after feeding an input  $\mathbf{u}_i$ , the output  $\tilde{\mathbf{u}}_0$  has a shape of  $h \times w \times N$  where N is the number of codebook items.
- (ii) We then apply a softmax function to convert all scores to a probability distribution for each token in the latent image. Afterwards we sample one token from each distribution using multinomial sampling according to the probability. The result  $\hat{\mathbf{u}}_0$  has a shape of  $h \times w$ .
- (iii) We randomly renoise a certain proportion of all sampled tokens back to their initial noise codebook values  $\mathbf{u}_T$ . This proportion is determined by the current timestep i.

A visual depiction of the sampling algorithm can be seen in Figure 3. Note that we do not renoise randomly and use the original noise tokens sampled at the beginning. We found this to lead to more robust outputs. Furthermore, unlike Chang *et al.*[4] we do not renoise the tokens with the lowest confidence and keep the ones with the highest scores, as this was not found to improve performance of our model. Instead, we renoise tokens randomly for the sake of simplicity.

Additionally, we employ two more techniques for improving the sampling process: The first is classifier-free-guidance (CFG) [18]. For CFG we introduce a null-label in the training. During sampling, we sample once with the null-label and once with the CLIP embedding as condition. Afterwards we linearly combine the two embeddings as

$$\mathbf{u_t} = \mathbf{u_{t,\emptyset}} + w \cdot (\mathbf{u_{t,c}} - \mathbf{u_{t,\emptyset}})$$

where w is a classifier weight that determines the pull towards the conditional sample. The second improvement is LTS [24] which was shown to be very successful in natural-language-processing. The main idea is inspired by information theory and states that high probability events do not induce high informational content. Instead, it is proposed to sample from areas in the probability distribution where the information content is close to the conditional entropy. We show the benefits of both, LTS and CFG in our ablation study in section 4.3.

#### 3.3 Token Predictor Architecture

Chang et al. use a bidirectional transformer for the image synthesis task. We argue that this has two main limiting factors: 1. Using a transformer necessitates treating the image as a flat 1D sequence, which is an unnatural projection of images and may impose a fundamental disadvantage during learning, since the 2D structure first needs to be learned through positional embeddings. 2. The quadratic memory growth limits transformers to small latent space resolutions, which in turn requires high compression rates. Furthermore, while autoregressive models rely on transformer architectures to function optimally and to have a large context window, our setup for training and sampling no longer requires a transformer and can be replaced by a convolutional model, which solves both aforementioned problems by having much lower memory requirements and induced 2D biases.

Our architecture is fully convolutional and consists of a U-Net-style [32] encoder-decoder structure utilizing residual blocks [13] (Figure 4). Next to the latent image, every block takes in the CLIP embedding and the timestep embedding. Instead of using standard 2D convolutions, we are using depthwise convolutions, since these are significantly faster and consume much less memory [19, 37]. Furthermore, each block also contains a linear projection, mapping both conditional embeddings to the latent dimension. Afterwards, we employ a modulated LayerNorm [22], which serves as the gateway for injecting and modulating the conditional information. This is followed by a channelwise convolution consisting of two fully connected layers combined via a GELU [14] activation. Finally, we scale the activations by a learned constant and add the residual connection. Figure 4 depicts the setup of our architecture vi-

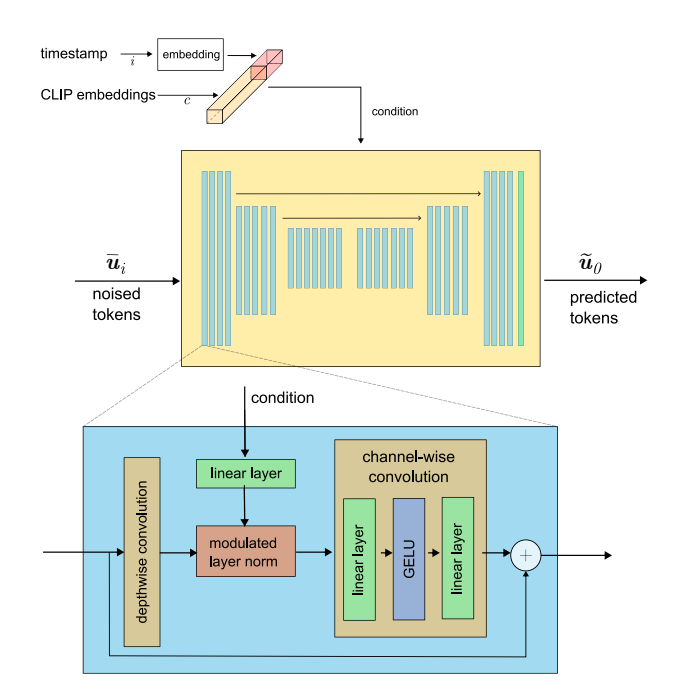


Figure 4: Visualisation of the model architecture of the token predictor.

sually. Note that our architecture is neither using attention, nor are we applying extensive normalization, making the model fast and memory-efficient.

#### 4 Experiments

Before training the final model, we conducted several low-scale experiments. For finding a suitable and efficient architecture, we trained on smaller latent space sizes, less model parameters and smaller datasets. After these initial experiments, we trained our full model, which we call *Paella*<sup>1</sup>. We empirically ground all of our design choices through the ablation studies and show our model's ability to perform text-conditional image synthesis and report about other out-of-the-box applications of our model.

#### 4.1 Architectural Search

For architectural optimization, we performed low-scale experiments using a latent space size of  $16 \times 16$ . The experiments were conducted on a small Flickr dataset for land-scapes<sup>2</sup>. The initial architecture used a kernel size k=7 and CLIP-, and timestep-mapping dimension of  $c_r=1024$ .

<sup>&</sup>lt;sup>1</sup>We decided to name the model after the popular food paella, because in our initial experiments generating food always was the first thing to work well

 $<sup>^2</sup>$ https://www.kaggle.com/datasets/arnaud58/landscape-pictures

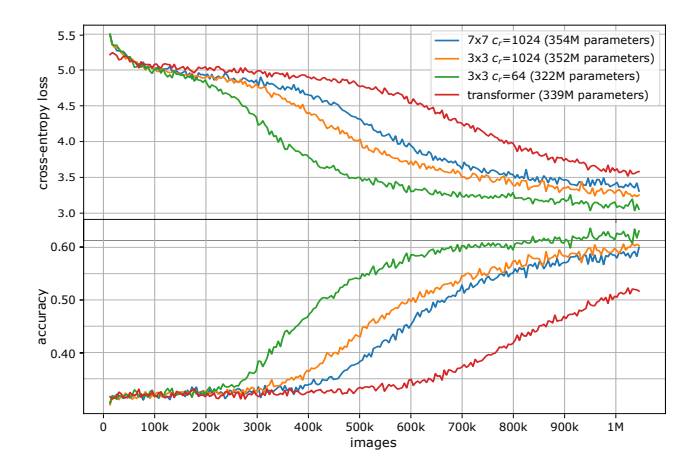


Figure 5: Comparison of different convolutional kernel configurations and a transformer as token predictors.

We first decreased the kernel size to k = 3 due to the fact that we work at small resolutions. By stacking many residual blocks the resulting receptive field can capture a global context well. Furthermore, embedding the timestep to the same dimension as the CLIP embedding is not necessary either, since it captures substantially less information. As a result, we decreased it to  $c_r = 64$  and observed not only a considerably lower number in total parameters, but also a significant increase in performance. To further proof our hypothesis that our proposal is superior to transformers, we trained an equally sized bidirectional transformer [4] on the same conditions as our convolutional experiments. This comparison can be seen in Figure 5. We observe that our model learns and converges significantly faster than the transformer approach, while both changes to the convolutional architecture also led to faster performance gains while at the same time reducing the overall parameter count.

#### 4.2 Training

After deciding on the overall architecture, we focused on the CLIP embedding. Using only image embeddings for training, as suggested by Ramesh *et al.*, requires the usage of a second model for enabling good text-to-image performance, mapping the text embedding to the image embedding. Hence, we decided to remove the need for such a prior and let the model directly learn from text embeddings. Incorporating all previous findings, we trained our largest model called *Paella* with 573M parameters. It was trained on 600 million images from the improved LAION-5B aesthetic [35] dataset for 600k steps with a batch size of 1408. Additionally, *Paella* also uses a larger CLIP ViT-G/14 [20]. We trained on 64 NVIDIA A100 for two weeks. All experiments use AdamW [23] for optimization with a learning

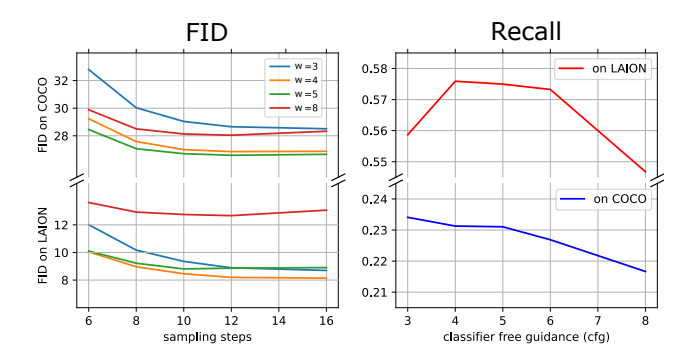


Figure 6: Evaluation of zero-shot Fréchet Inception Distance (FID) [15] vs. the classifier-free guidance weight w (left) and recall [21] (right) on the COCO and LAION dataset. Recall evaluation uses 12 sampling steps. All evaluations use mixed-precision.

rate of  $3e^{-4}$  using a linear warm-up schedule for 30k steps.

#### 4.3 Text-Conditional Image Synthesis

To demonstrate Paella's text-conditional image generation capabilities we provide visual results (see Figure 1), but also quantitative numerical analysis. We evaluated zeroshot Fréchet Inception Distance (FID) [15] scores to determine the faithfulness and fidelity compared to ground truth images from MS COCO [6]. Although being widely used for this purpose, we argue that COCO may not represent the best choice to evaluate general-purpose text-to-image models. COCO primarily contains depictions of realistic everyday situations and generally lacks artistic images, fictional content, creative concepts etc. As a result, we propose a carefully crafted subset of the LAION aesthetic dataset [35], which we refer to as LAION-30k, consisting of 30.000 images and captions with a lot of variety and diversity. The dataset, as well as a description of how the dataset was created, can be found in section A of the supplemental material. Next to FID calculations, we also evaluate precision & recall [21] for measuring the distributional coverage on both COCO-30k and LAION-30k. We evaluate against different hyperparameter settings for the number of timesteps T and CFG weight w. The results can be found in Figure 6 and the supplemental section B. We find the FID metric to be significantly higher when evaluated on the COCO dataset compared to the LAION-30k evaluation set, and both precision and recall considerably lower. While the samples from the LAION subset had been seen during training once, we are confident that no overfitting ocurred (see section A of the supplemental material). Table 1 shows a comparison to current state-of-the-art methods. We find that the performance on COCO is worse than most other models.

However, our model has the great benefit of needing a

Model	Parameters	Sampling Steps	FID-COCO-30k	FID-LAION-30k
DALL-E [30]	12B	256	~28	-
CogView [30]	4B	1024	27.1	-
Parti [43]	20B	1024	7.23	-
GLIDE [25]	3.5B	250	12.24	-
Make-A-Scene [12]	4B	1024	11.84	-
DALL-E 2 [29]	3.5B	250	10.39	-
Imagen [34]	2B	1000	7.27	-
Stable-Diffusion v1.4 @ 256 × 256 [31]	860M	50	25.40*	10.81*
Paella wo/CFG + wo/LTS			106.63	57.59
Paella wo/CFG + w/LTS	573M	12	33.24	30.71
Paella w/CFG + wo/LTS			30.90	9.82
Paella w/CFG + wo/LTS (proposed)			26.72	8.20

Table 1: Comparison to other state-of-the-art text-to-image methods, including an ablation study of our *Paella* model with (w/) and without (wo/) classifier-free guidance (CFG) and locally typical sampling (LTS). \*: own evaluation, generated with 50 DDIM [17] steps and w=7.5 at  $512\times512$ , downsampled to  $256\times256$ .

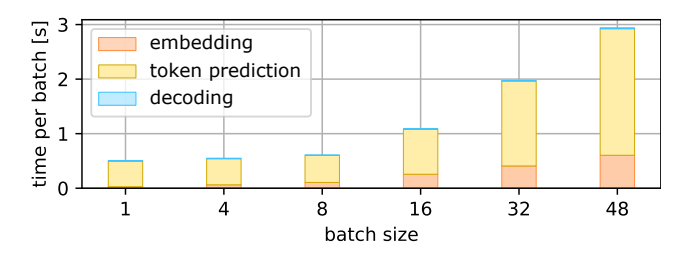


Figure 7: Inference wall-clock runtime of our model vs. the batch size on an NVIDIA A100 GPU (8 steps, mixed precision, text-to-image task).

fraction of sampling steps in contrast to other methods. In combination with the inference speed of each step (due to the use of the CNN), Paella can sample high quality images in before unseen times. In Figure 7 we show inference speeds given different batch sizes on a single NVIDIA A100. The model is able to sample 48 images in 2.94 seconds. After finding suitable values for T and w we compare if CFG and LTS are beneficial or detrimental for image generations. The results of this ablation study can be seen in Table 1 as well. We find that using CFG and LTS is extremely valuable, resulting in a 586% and 187% improvement on LAION-30k, respectively.

#### 4.4 Image Manipulations

The design choices of our architecture and the specific way of conditioning unfold many possibilities for image synthesis tasks. Conditioning on CLIP enables us to generate variations of images, interpolate in the latent space and perform structural edits between images. Moreover, since our model is fully convolutional, this naturally allows for sampling at any resolution, inpainting and outpainting of images. Last but not least, our procedure of conditioning enables us to condition different tokens on different embeddings.

#### 4.4.1 Image Variations



Figure 8: Results from the finetuned *Paella* on image embeddings. The leftmost image depicts the ground truth and the adjacent images are the generated variations.

Since *Paella* was solely trained on text embeddings, conditioning the model on image embeddings from CLIP doesn't work sufficiently and results in repeating simple patterns of the conditioned image. In order to still use our model for this task, we finetune for 40k steps on image embeddings extracted from the visual part of CLIP. After finetuning, we can extract the image embedding from a given image and feed this to *Paella* for sampling. The resulting outputs are semantically very similar to the original image, however naturally have some distinct differences (position, alignment, scale, etc.) (Figure 8).

#### 4.4.2 Image Inpainting & Outpainting



Detailed realistic painting of a clock tower in the style of starry night.

Aerial view of a beautiful nature landscape.

Figure 9: Visual samples for outpainting images. The dashed rectangle depicts the original image, which is outpainted conditioned on the prompt given below the image.

The convolutional nature of *Paella* allows us to generate latent images at any size. Unlike with transformer models, we are not restricted to a context window and hence do not need to use shifting context windows to sample larger



Figure 10: Example inpainted images with our model. Dashed rectangles showcase areas to be filled in by conditioning on text-prompts, while the rest of the image will be kept fixed.

images. This property can be used for outpainting images, which refers to extending an existing image in any direction and filling in semantically correct context. We proceed as follows: First, we encode an existing image to token space using the VQGAN encoder. For instance, an image with a height and width of 256×256 is encoded to a latent image with spatial resolution of  $32 \times 32$ . Next, we extend the image in the desired directions (e.g.,  $32 \times 64$  increases the image in the horizontal direction). The newly added tokens are initialized randomly. Subsequently, we start sampling as usual with the only difference being that after each iteration, we reset the original image tokens back to their initial values and only keep the extended tokens. In addition to semantically extending an image, we can also replace and fill in existing content based on a textual prompt, which we refer to as inpainting. The overall procedure is similar to outpainting. We first define a mask in the latent space for tokens which should be resampled. Then we start sampling and after each iteration only keep the tokens at the inpainted positions. Figure 9 and Figure 10 show examples of inpainting and outpainting with Paella, respectively.

## 4.4.3 Latent Space Interpolation

Due to the fact that the CLIP space is continuous, it is possible to interpolate between points and sample along their trajectory. This results in smoothly transitioning between the concepts and semantics of images. Many sophisticated methods could be applied for generating the trajectory, however we found satisfactory results by simply using linear interpolations. Figure 11 shows examples of this.

## 4.4.4 Structural Editing

We define structural morphing as the act of changing an existing image semantic content while keeping the overall structure of the image the same. Figure 5 shows examples of this. We achieve this editing by encoding the base image to its latent representation followed by noising a certain amount of tokens (e.g., 75%). We feed this representation as the initial input to the sampling process together with the conditional embedding. Another important change is to use a later starting point for the time embedding (t>0), to indicate that the image is not full noise.

## 4.4.5 Multi-Conditioning

The process of conditioning our model happens through the modulated layer normalization, which is denormalized with the projected CLIP embedding afterwards. The processed embedding must be of the same dimensionality as the latent image. Conditioning on a single embedding is achieved by expanding the projection to the same latent size as the image. However, we are free choose different embeddings for different parts of the image. Theoretically, every single token can be conditioned on a distinct embedding than all others. This freedom of conditioning permits us to generate 'story-telling' images. For example we can sample a wide image where the left side is conditioned on 'the army was marching through the fields', while the right side is conditioned on 'the castle was protected by a two headed dragon' (see Fig. 13 for visual examples).

#### 5 Discussion & Limitations

The numerical evaluation of our model reveals that on the LAION-30k evaluation set, our model yields lower FID scores than resampled images of Stable Diffusion<sup>3</sup>. Visually, this, however, does not coincide with an improved image quality over the competing model. As pointed out by Shmelkov et al., FID does not capture image quality directly, but estimates it using the feature distance of original and generated images, modelled as Gaussian distributions as a proxy [36]. Optimally, the trained feature extractor generates features that are the most discriminative for the class differentiation and hence also are subject to the class distribution of the dataset. This means that the FID is not only highly dependent on the feature extractor (typically Inception V2/V3 [39]) but also the dataset used for training it (typically ImageNet [33]). Likewise, the training objective (classification) does not necessarily yield features of highest discrimination for image composition or perceived image quality. Additionally, FID incorporates a strong dependency on the dataset that is used for evaluation, as also confirmed by our results. The data distribution, which is notably different on COCO and LAION, may result in a different distribution of features and thus impact the FID

 $<sup>^3</sup>$  Stable diffusion originally outputs  $512\times512$  images, hence, for the comparison we downsampled the generated images to  $256\times256.$ 

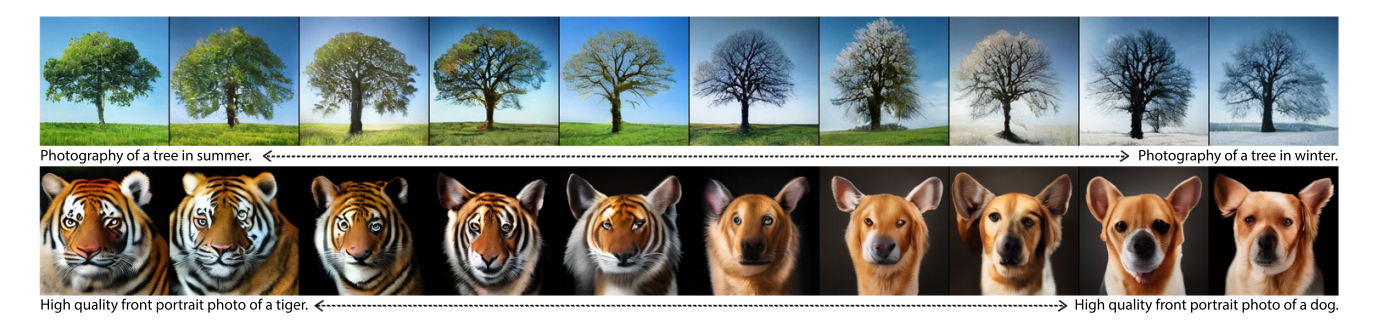


Figure 11: Linear Interpolations between different captions in the CLIP embedding space. We use a fixed seed for sampling each image.



Figure 12: Structural editing refers semantically changing the content of the image while preserving the overall colours and shape.

score either positively or negatively. In the case of Paella, the penalty for the evaluation on COCO may also have been caused by the vector quantizer of our architecture. As the distribution of patterns for the VQGAN is subject to the distribution within the dataset, the FID might be improved by retraining the VQGAN on the target dataset (COCO). A further limiting factor might be that our model was trained with text conditioning only. Since text-embeddings contain much less information than image embeddings, this can result in a lower data space coverage. This could have disproportionally impacted the evaluation on the different dataset, due to the lower support of certain conditions during training caused by the distribution shift.

The quantized latent spaces, while providing the favorable properties we described in this work, also comes with drawbacks compared to diffusion-based models: Since we perform noising of the discrete tokens from a uniform distribution, each noising removes the complete information at the position of the noised token. We thus can't perform continuous denoising of an image on a microscopic level, which also restricts applications using smooth transitions in the latent space, such as structural editing.

One central limitation of our evaluation is the parameter and training steps difference between *Paella* and other state-of-the-art models. The amount of images other mod-



Figure 13: Depictions of conditioning generations on different textual prompts in a single sampling cycle. The dashed lines separate different textual conditions.

els have seen during training outweighs our experiments by magnitudes, which makes fair comparisons hard, especially when many of these models are kept private. To this degree, we hope to make a contribution to reproducible and transparent science in our field by providing the complete model including all weights.

## 6 Conclusion

In this work we presented *Paella*, a text-to-image generation system using a novel training objective, an improved sampling strategy and a fully-convolutional architecture. We showed that our model can generate high-fidelity images despite being substantially smaller and requiring less steps for sampling than existing models while still reaching competitive numerical results. In addition to *Paella's* abilities to model relationships from the textual into the image domain, its specific architecture and conditioning strat-

egy allows for a variety of image manipulations tasks such as inpainting, outpainting, variations, etc. We especially want to highlight the simple and straightforward setup of this model regarding training and sampling procedure compared to models based on diffusion or transformers and believe this method will make generative techniques more accessible to a variety of people, even outside the generative research field, which we argue will become crucial as this technology progresses further.

## Reproducibility and data availability

We provide all model weights of our final model Paella, together with a pytorch-based implementation within our github repository<sup>4</sup>. Further, we provide training scripts and inference notebooks to support reproducibility of our findings.

## Acknowledgements

The authors wish to express their thanks to Stability AI Inc. for providing generous computational resources for our experiments and LAION gemeinnütziger e.V. for dataset access and support.

#### References

- [1] Martin Arjovsky and Léon Bottou. Towards principled methods for training generative adversarial networks. In *Proceedings of the International Conference on Learning Representations (ICLR)*, 2017.
- [2] Sanjeev Arora, Rong Ge, Yingyu Liang, Tengyu Ma, and Yi Zhang. Generalization and equilibrium in generative adversarial nets (GANs). In *International Conference on Machine Learning*, pages 224–232. PMLR, 2017.
- [3] Andrew Brock, Jeff Donahue, and Karen Simonyan. Large scale GAN training for high fidelity natural image synthesis. In *International Conference on Learning Prepresenta*tions (ICLR), 2019.
- [4] Huiwen Chang, Han Zhang, Lu Jiang, Ce Liu, and William T Freeman. MaskGIT: Masked generative image transformer. In Proceedings of the IEEE/CVF Conference on Computer Vision and Pattern Recognition, pages 11315–11325, 2022.
- [5] Mark Chen, Alec Radford, Rewon Child, Jeffrey Wu, Heewoo Jun, David Luan, and Ilya Sutskever. Generative pretraining from pixels. In *International Conference on Machine Learning*, pages 1691–1703. PMLR, 2020.
- [6] Xinlei Chen, Hao Fang, Tsung-Yi Lin, Ramakrishna Vedantam, Saurabh Gupta, Piotr Dollár, and C Lawrence Zitnick. Microsoft COCO captions: Data collection and evaluation server. arXiv preprint arXiv:1504.00325, 2015.

- [7] Prafulla Dhariwal and Alexander Nichol. Diffusion models beat gans on image synthesis. Advances in Neural Information Processing Systems, 34:8780–8794, 2021.
- [8] Ming Ding, Zhuoyi Yang, Wenyi Hong, Wendi Zheng, Chang Zhou, Da Yin, Junyang Lin, Xu Zou, Zhou Shao, Hongxia Yang, et al. Cogview: Mastering text-to-image generation via transformers. Advances in Neural Information Processing Systems, 34:19822–19835, 2021.
- [9] Ming Ding, Wendi Zheng, Wenyi Hong, and Jie Tang. Cogview2: Faster and better text-to-image generation via hierarchical transformers. arXiv preprint arXiv:2204.14217, 2022.
- [10] Alexey Dosovitskiy, Lucas Beyer, Alexander Kolesnikov, Dirk Weissenborn, Xiaohua Zhai, Thomas Unterthiner, Mostafa Dehghani, Matthias Minderer, Georg Heigold, Sylvain Gelly, et al. An image is worth 16x16 words: Transformers for image recognition at scale. In *Proceedings of* the International Conference on Learning Representations (ICLR), 2020.
- [11] Patrick Esser, Robin Rombach, and Bjorn Ommer. Taming transformers for high-resolution image synthesis. In *Proceedings of the IEEE/CVF Conference on Computer Vision and Pattern Recognition*, pages 12873–12883, 2021.
- [12] Oran Gafni, Adam Polyak, Oron Ashual, Shelly Sheynin, Devi Parikh, and Yaniv Taigman. Make-a-scene: Scene-based text-to-image generation with human priors. *arXiv* preprint arXiv:2203.13131, 2022.
- [13] Kaiming He, Xiangyu Zhang, Shaoqing Ren, and Jian Sun. Deep residual learning for image recognition. In *Proceedings of the IEEE Conference on Computer Vision and Pattern Recognition*, pages 770–778, 2016.
- [14] Dan Hendrycks and Kevin Gimpel. Gaussian error linear units (GELUs). arXiv preprint arXiv:1606.08415, 2016.
- [15] Martin Heusel, Hubert Ramsauer, Thomas Unterthiner, Bernhard Nessler, and Sepp Hochreiter. GANs trained by a two time-scale update rule converge to a local nash equilibrium. Advances in Neural Information Processing Systems, 30, 2017.
- [16] Jonathan Ho, Ajay Jain, and Pieter Abbeel. Denoising diffusion probabilistic models. *Advances in Neural Information Processing Systems*, 33:6840–6851, 2020.
- [17] Jonathan Ho, Ajay Jain, and Pieter Abbeel. Denoising diffusion probabilistic models. *Advances in Neural Information Processing Systems*, 33:6840–6851, 2020.
- [18] Jonathan Ho and Tim Salimans. Classifier-free diffusion guidance. arXiv preprint arXiv:2207.12598, 2022.
- [19] Andrew G. Howard, Menglong Zhu, Bo Chen, Dmitry Kalenichenko, Weijun Wang, Tobias Weyand, Marco Andreetto, and Hartwig Adam. Mobilenets: Efficient convolutional neural networks for mobile vision applications. arXiv preprint arXiv:1704.04861, 2017.
- [20] Gabriel Ilharco, Mitchell Wortsman, Nicholas Carlini, Rohan Taori, Achal Dave, Vaishaal Shankar, Hongseok Namkoong, John Miller, Hannaneh Hajishirzi, Ali Farhadi, and Ludwig Schmidt. OpenCLIP. Zenodo, July 2021.
- [21] Tuomas Kynkäänniemi, Tero Karras, Samuli Laine, Jaakko Lehtinen, and Timo Aila. Improved precision and recall met-

<sup>4</sup>https://github.com/dome272/Paella

- ric for assessing generative models. Advances in Neural Information Processing Systems, 32, 2019.
- [22] Kwonjoon Lee, Huiwen Chang, Lu Jiang, Han Zhang, Zhuowen Tu, and Ce Liu. ViTGAN: Training GANs with vision transformers. arXiv preprint arXiv:2107.04589, 2021.
- [23] Ilya Loshchilov and Frank Hutter. Decoupled weight decay regularization. *International Conference on Learning Rep*resentations (ICLR), 2019.
- [24] Clara Meister, Tiago Pimentel, Gian Wiher, and Ryan Cotterell. Locally typical sampling. arXiv preprint arXiv:2202.00666, 2022.
- [25] Alex Nichol, Prafulla Dhariwal, Aditya Ramesh, Pranav Shyam, Pamela Mishkin, Bob McGrew, Ilya Sutskever, and Mark Chen. Glide: Towards photorealistic image generation and editing with text-guided diffusion models. arXiv preprint arXiv:2112.10741, 2021.
- [26] Alec Radford, Jong Wook Kim, Chris Hallacy, Aditya Ramesh, Gabriel Goh, Sandhini Agarwal, Girish Sastry, Amanda Askell, Pamela Mishkin, Jack Clark, et al. Learning transferable visual models from natural language supervision. In *International Conference on Machine Learning*, pages 8748–8763. PMLR, 2021.
- [27] Alec Radford, Jeffrey Wu, Rewon Child, David Luan, Dario Amodei, Ilya Sutskever, et al. Language models are unsupervised multitask learners. *OpenAI blog*, 1(8):9, 2019.
- [28] Colin Raffel, Noam Shazeer, Adam Roberts, Katherine Lee, Sharan Narang, Michael Matena, Yanqi Zhou, Wei Li, Peter J Liu, et al. Exploring the limits of transfer learning with a unified text-to-text transformer. *J. Mach. Learn. Res.*, 21(140):1–67, 2020.
- [29] Aditya Ramesh, Prafulla Dhariwal, Alex Nichol, Casey Chu, and Mark Chen. Hierarchical text-conditional image generation with CLIP latents. arXiv preprint arXiv:2204.06125, 2022.
- [30] Aditya Ramesh, Mikhail Pavlov, Gabriel Goh, Scott Gray, Chelsea Voss, Alec Radford, Mark Chen, and Ilya Sutskever. Zero-shot text-to-image generation. In *International Confer-ence on Machine Learning*, pages 8821–8831. PMLR, 2021.
- [31] Robin Rombach, Andreas Blattmann, Dominik Lorenz, Patrick Esser, and Björn Ommer. High-resolution image synthesis with latent diffusion models. In *Proceedings of the IEEE/CVF Conference on Computer Vision and Pattern Recognition*, pages 10684–10695, 2022.
- [32] Olaf Ronneberger, Philipp Fischer, and Thomas Brox. Unet: Convolutional networks for biomedical image segmentation. In *International Conference on Medical Image Computing and Computer-Assisted Intervention*, pages 234–241. Springer, 2015.
- [33] Olga Russakovsky, Jia Deng, Hao Su, Jonathan Krause, Sanjeev Satheesh, Sean Ma, Zhiheng Huang, Andrej Karpathy, Aditya Khosla, Michael Bernstein, et al. Imagenet large scale visual recognition challenge. *International Journal of Computer Vision*, 115(3):211–252, 2015.
- [34] Chitwan Saharia, William Chan, Saurabh Saxena, Lala Li, Jay Whang, Emily Denton, Seyed Kamyar Seyed Ghasemipour, Burcu Karagol Ayan, S Sara Mahdavi, Rapha Gontijo Lopes, et al. Photorealistic text-to-image

- diffusion models with deep language understanding. arXiv preprint arXiv:2205.11487, 2022.
- [35] Christoph Schuhmann, Romain Beaumont, Richard Vencu, Cade Gordon, Ross Wightman, Mehdi Cherti, Theo Coombes, Aarush Katta, Clayton Mullis, Mitchell Wortsman, et al. Laion-5b: An open large-scale dataset for training next generation image-text models. arXiv preprint arXiv:2210.08402, 2022.
- [36] Konstantin Shmelkov, Cordelia Schmid, and Karteek Alahari. How good is my gan? In Proceedings of the European Conference on Computer Vision (ECCV), pages 213– 229, 2018.
- [37] Laurent Sifre and Stéphane Mallat. Rigid-motion scattering for texture classification. arXiv preprint arXiv:1403.1687, 2014.
- [38] Jascha Sohl-Dickstein, Eric Weiss, Niru Maheswaranathan, and Surya Ganguli. Deep unsupervised learning using nonequilibrium thermodynamics. In *International Confer*ence on Machine Learning, pages 2256–2265. PMLR, 2015.
- [39] Christian Szegedy, Wei Liu, Yangqing Jia, Pierre Sermanet, Scott Reed, Dragomir Anguelov, Dumitru Erhan, Vincent Vanhoucke, and Andrew Rabinovich. Going deeper with convolutions. In Proceedings of the IEEE Conference on Computer Vision and Pattern Recognition, pages 1–9, 2015.
- [40] Aaron Van Den Oord, Oriol Vinyals, et al. Neural discrete representation learning. Advances in Neural Information Processing Systems, 30, 2017.
- [41] Ashish Vaswani, Noam Shazeer, Niki Parmar, Jakob Uszkoreit, Llion Jones, Aidan N Gomez, Łukasz Kaiser, and Illia Polosukhin. Attention is all you need. Advances in Neural Information Processing Systems, 30, 2017.
- [42] Zihao Wang, Wei Liu, Qian He, Xinglong Wu, and Zili Yi. Clip-gen: Language-free training of a text-to-image generator with clip. arXiv preprint arXiv:2203.00386, 2022.
- [43] Jiahui Yu, Yuanzhong Xu, Jing Yu Koh, Thang Luong, Gunjan Baid, Zirui Wang, Vijay Vasudevan, Alexander Ku, Yinfei Yang, Burcu Karagol Ayan, Ben Hutchinson, Wei Han, Zarana Parekh, Xin Li, Han Zhang, Jason Baldridge, and Yonghui Wu. Scaling autoregressive models for content-rich text-to-image generation. arXiv preprint arXiv:2206.10789, 2022.

## Part I

# **Supplemental Material**

#### A Evaluation subset for LAION-5B

We hypothesize that using a subset of COCO [6] to evaluate general purpose text-to-image models is not a good estimator of a model's capabilities in terms of image quality, fidelity and generalization, due to a strong dependency on dataset distribution for most metrics. The COCO dataset only contains realistic all-day situations and does not include most other categories appearing in commonly used training datasets like arts, imagination, abstract concepts, knowledge of people & the world etc. Therefore, we propose a more suitable evaluation dataset for this purpose which we call LAION-30k. This dataset is a subset of the LAION improved aesthetic [35] corpus. This dataset contains a tremendous amount of variability and diversity and covers a large number of topics, categories, styles, and contains a lot of world knowledge. While this dataset already is a filtered and cleaned subset of the LAION-5B dataset [35] in terms of predicted image aesthetic scores, there still exist many low-quality images and an even higher number of low-informational captions (containing, e.g., websites, noise, file names, random numbers etc.). Therefore, we suggest to use a more carefully filtered subset, considering also the quality of captions.

At first we set a higher threshold for the aesthetic score and only considered images with a score > 6. Afterwards we employed a two-fold caption cleaning process of first checking if the captions meet any exclusion criteria and, if not, a subsequent purification. The criteria we used to check for exclusion are:

- · too short or too long captions
- captions containing any special characters such as underscores or semicolons
- captions with non-ascii letters
- · URLs or numbers
- captions with specific words (e.g., related to questions or to specific data providers)

The subsequent cleaning consisted of removing multiple whitespaces and quotation marks. We find that using this protocol leads to a removal of most of the noisy captions and images an hence results in an increased quality for both captions and images of the evaluation set. Due to copyright issues, we can not provide a direct download for the images, but we provide scripts to replicate our proposal in our github repository.

#### Investigating the likelihood for overfitting

In order to exclude the possibility that the low FID values on the LAION-30k dataset were achieved by overfitting to the training data, even though each sample had only been seen once, we also visually compared the generations of the model to the closest images of the LAION-30k dataset.

For this, we employed a k nearest neighbor approach between the encoded representations of the dataset and the generated images using CLIP [26] image embeddings. We then visually compared the generated image to the nearest neighbors in latent space. If overfitting occured, then the sampled images from a specific caption should be reasonably close to the ground truth or other images from the same dataset. We found no such relation in numerous random picks. In fact, we found that the images are very distinct even though conveying the same semantic content. Unfortunately, due to the LAION dataset containing a significant proportion of images with unclear copyright situation, we can't provide these comparisons as part of this supplementary material.

# **B** Additional evaluation metrics

To investigate variability of generated images, besides the recall we also evaluated the precision [21].

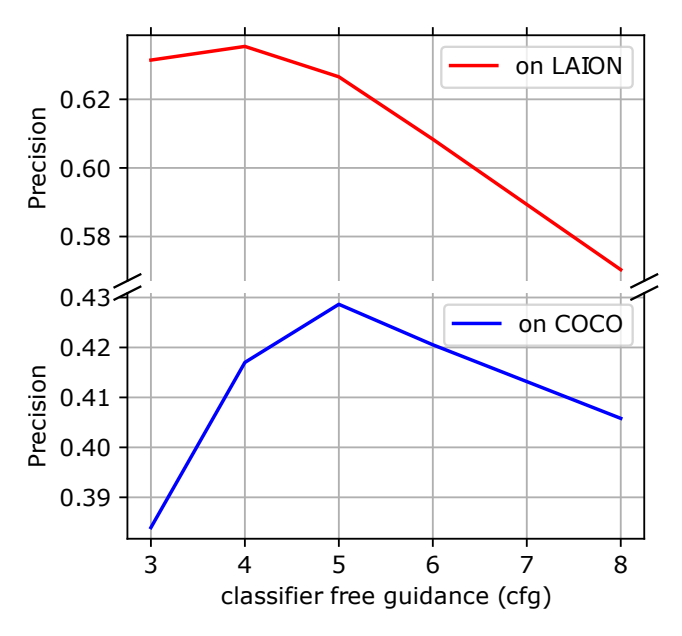


Figure S14: Precision of our model when evaluated on MS COCO or the LAION subset presented in section A of the supplementary material. Twelve sampling steps were used.